

Version dated: November 7, 2025

Nonparametric Modeling of Continuous-Time Markov Chains

FILIPPO MONTI¹

XIANG JI²

MARC A. SUCHARD^{1,3,4}

¹ *Department of Biostatistics, Jonathan and Karin Fielding School of Public Health,
University of California Los Angeles, Los Angeles, CA, USA*

² *Department of Mathematics, Tulane University, New Orleans, LA, USA*

³ *Department of Biomathematics, David Geffen School of Medicine at UCLA, University of
California Los Angeles, Los Angeles, CA, USA*

⁴ *Department of Human Genetics, David Geffen School of Medicine at UCLA, University of
California Los Angeles, Los Angeles, CA, USA*

Corresponding author: Marc A. Suchard, Departments of Biostatistics, Biomathematics, and Human Genetics, University of California Los Angeles, 695 Charles E. Young Dr., South, Los Angeles, CA 90095-7088, USA; E-mail: msuchard@ucla.edu

Abstract Inferring the infinitesimal rates of continuous-time Markov chains (CTMCs) is a central challenge in many scientific domains. This task is hindered by three factors: quadratic growth in the number of rates as the CTMC state space expands, strong dependencies among rates, and incomplete information for many transitions. We introduce a new Bayesian framework that flexibly models the CTMC rates by incorporating covariates through Gaussian processes (GPs). This approach improves inference by integrating new information and contributes to the understanding of the CTMC stochastic behavior by shedding light on potential external drivers. Unlike previous approaches limited to linear covariate effects, our method captures complex non-linear relationships, enabling fuller use of covariate information and more accurate characterization of their influence. To perform efficient inference, we employ a scalable Hamiltonian Monte Carlo (HMC) sampler. We address the prohibitive cost of computing the exact likelihood gradient by integrating the HMC trajectories with a scalable gradient approximation, reducing the computational complexity from $\mathcal{O}(K^5)$ to $\mathcal{O}(K^2)$, where K is the number of CTMC states. Finally, we demonstrate our method on Bayesian phylogeography inference—a domain where CTMCs are central—showing effectiveness on both synthetic and real datasets.

Keywords: Bayesian inference, Gaussian process, Hamiltonian Monte Carlo, approximate gradient, phylogenetics

1 Introduction

Continuous-time Markov chains (CTMCs) are a probabilistic modeling tool used in a wide range of fields such as phylogenetics, epidemiology, survival analysis, and biochemistry (Jukes and Cantor, 1969; Kalbfleisch and Lawless, 1985). A CTMC is a stochastic process that randomly transitions between discrete states over continuous time. The transitions occur at exponentially distributed waiting times, and the future state depends only on the present state, not on the past (Markov property). The parameters describing the CTMC can be collected into a matrix called an *infinitesimal rate matrix* or generator. A key inferential task to understand the CTMC dynamics is, therefore, estimating the entries (rates) of such a matrix. This is challenging since the number of rates increases quadratically with the number of discrete states and the data might not carry information on transitions between all pairs of states.

Direct parametrization One approach to reducing the number of free parameters in the rate matrix is to impose structural restrictions. This method has been particularly effective in fields such as evolutionary biology, where a lower-dimensional parametrization can be motivated by knowledge of the underlying biological dynamics. A rich body of literature has explored DNA substitution processes, proposing and testing various constraints (Jukes and Cantor, 1969; Kimura, 1980).

Direct parametrization, however, becomes less effective when the underlying jump process is not well studied. This issue is exacerbated as the state space grows, since, in the absence of prior knowledge, multiple parametrizations must be explored. This, in turn, introduces a model selection problem whose complexity increases combinatorially with the size of the state space.

Use of covariates Another modeling technique leverages pre-existing information captured by *covariates*. One upside of this approach is that, as a byproduct, it sheds light on whether and how those covariates influence the CTMC jumping process. For instance, phylogeography explores the emergence and dispersal of biological entities, including pathogenic viruses, using CTMCs (Pybus et al., 2012; Lemey et al., 2014). The rate of a viral infection spreading from one country to another is likely dependent on the distance that separates the two countries as well as their population sizes.

Within a frequentist framework, Kalbfleisch and Lawless (1985) proposed to study the relationship between covariates and rates based on a log-linear model. This approach was then extended to a Bayesian setting in the context of phylogeography. Motivated by a rich set of examples, researchers have actively contributed to the improvement of these models. Nonetheless, the geographic locations under study tend to be high in number, and finding a credible direct parametrization that describes the movement among them remains challenging.

Bayesian Inference Bayesian methods have proven to be particularly well-suited for inferring CTMCs, especially when the state space is large and when simultaneous inference is essential as the CTMC is part of a larger model. In such cases, the data may provide weak or no information for certain rate parameters. Consequently, the use of prior distributions provides a crucial means of regularization and improved inference.

Sampling There has been a flourishing literature on Markov chain Monte Carlo (MCMC) techniques (Metropolis et al., 1953; Hastings, 1970) to sample from the posterior distribution of CTMC rates (Suchard et al., 2001). However, when the state space is large, employing a simple Metropolis-Hastings-based MCMC for sampling rates becomes challenging, not only due to their high dimensionality but also because their strong mutual dependencies hinder efficient exploration of the parameter space. Adopting a Hamil-

tonian Monte Carlo (HMC)-based sampling scheme (Neal, 2011) has proven to be an effective solution for sampling high-dimensional and highly dependent parameters. For instance, in the context of CTMCs, Zhao et al. (2016) use HMC to sample rates based on a Bayesian log-linear model.

Our proposal In this work we introduce a new Bayesian framework that flexibly models CTMC rates by incorporating covariate relationships through Gaussian processes (GPs). This approach relaxes the restrictive log-linear form of existing models, enabling the capture of complex nonlinear relationships. GPs can represent a broad range of functional forms, allowing us to fully leverage covariate information and more accurately characterize their effects.

A major challenge of HMC-based sampling for many CTMC models is the repeated computation of the (log-) likelihood gradient with respect to the parameters of interest. For partially observed CTMCs, this involves evaluating multiple matrix exponential derivatives (computational complexity $\mathcal{O}(K^3)$) for each of the infinitesimal rates ($\mathcal{O}(K^2)$), leading to a total complexity of $\mathcal{O}(K^5)$ operations and creating a severe computational bottleneck even for moderately-sized state spaces. To address this, we explore an approximation of the matrix exponential gradient that reduces the overall cost to only $\mathcal{O}(K^2)$ (Didier et al., 2024), gaining a three orders-of-magnitude improvement. Crucially, using an approximate gradient does not hinder HMC convergence, as supported by the literature on HMC using surrogate trajectories (Li et al., 2019). Finally, we adapt the proposed methods to Bayesian phylogeographic inference following Magee et al. (2024), and demonstrate how the aforementioned approximation is even more critical for efficient sampling under flexible GP modeling assumptions.

Structure of the paper This paper is structured as follows: Sections 2 and 3 present our proposed methodology, followed by an application to phylogeography in Section 4 and

concluding discussion in Section 5. More specifically, Section 2 presents the likelihood and the prior choices. We begin with a brief introduction on CTMCs (2.1), then derive the joint distribution of the observed data under different sampling scenarios, distinguishing between fully and partially observed CTMCs (2.2). We also motivate the use of GPs as a prior on the rate matrix (2.3). Section 3 addresses inference. It opens with an overview justifying the use of HMC with surrogate trajectories as our reference sampler. For partially observed data, we show how the likelihood gradient can be computed efficiently using the aforementioned approximation of the matrix exponential gradient. Section 4 then extends the proposed framework to data with a tree-structured dependency, a setting of central importance in phylogeography. Finally, we demonstrate the performance of our models on synthetic and real datasets, and we estimate empirically the scalability of the gradient approximation versus its exact counterpart (4.4).

2 Methods I: Likelihood and prior

2.1 Brief introduction to continuous-time Markov chains

A (time-homogeneous) CTMC on a finite state space $\mathbf{S} = \{s_1, \dots, s_K\}$ ($|\mathbf{S}| = K$) is a stochastic process $\{Y(t) : t \in \mathbb{R}^+\}$ taking values in \mathbf{S} and defined by the following two components

1. an *initial distribution* $\boldsymbol{\pi}^*$ on \mathbf{S} so that for all $i \in \mathbf{S}$, $\mathbb{P}(Y(0) = i) = \pi_i^*$,
2. an *infinitesimal rate matrix* $\mathbf{Q} = (q_{ij})_{i,j \in \mathbf{S}}$ with non-negative off-diagonal elements ($q_{ij} \geq 0$ for $i \neq j$), and with the diagonal elements constrained so that each row of \mathbf{Q} sums to zero, or $q_{ii} = -\sum_{j \neq i} q_{ij}$ for every $i \in \mathbf{S}$. Moreover, for all pairs of states $i, j \in \mathbf{S}$, every $t \in \mathbb{R}^+$ such that $\mathbb{P}(Y(t) = i) > 0$ then, for small

values $h > 0$:

$$\mathbb{P}(Y(t+h) = j | Y(t) = i) = \mathbb{1}(i = j) + q_{ij}h + o(h) \quad (1)$$

where $\mathbb{1}(\cdot)$ is the indicator function. Following a well-established convention, we adopt $q_i = -q_{ii} \geq 0$ to refer to the absolute value of the diagonal elements.

More intuitively, if the CTMC Y_t starts at some state i , it will leave such state after an exponentially distributed time with rate q_i (*time* component) and will jump to a different state j with probability $\frac{q_{ij}}{q_i}$ (*location* component).

The exponential random variable describing the time spent in a state i before leaving it has been assigned several names; in this work, we refer to it as the *waiting time*, W_i . In addition, we denote the realized value of the CTMC $Y(t)$ at time t with $y(t)$. If we assume the CTMC is observed N times, then we refer to the vector of observations as $\mathbf{y} = (y_1, y_2, \dots, y_N)$. Similarly, we refer to the times when each value y_i is observed as t_i ; we also collect those values in the vector $\mathbf{t} = (t_1, t_2, \dots, t_N)$.

2.2 Joint distribution of the observed data

2.2.1 Fully observed data

The simplest scenario involves fully observed data during an interval, say $[0, t]$. Specifically, we assume that the CTMC *only* jumps at times t_1, t_2, \dots, t_N . Therefore, we can write the joint distribution of (\mathbf{y}, \mathbf{t}) :

$$p(\mathbf{y}, \mathbf{t} | \mathbf{Q}, \text{fully observed}) = \pi^*(y_1) \prod_{i=2}^N \left[\mathbb{P}(W_{y_i} = t_i - t_{i-1}) \frac{q_{y_{i-1}, y_i}}{q_{y_i}} \right], \quad (2)$$

under the restriction that $t_N = t$. In this formula, we are traversing the CTMC path along $[0, t]$ by iteratively multiplying the probability of the waiting times and of the

jumps to each specific state.

2.2.2 Partially observed data

A more realistic scenario involves a partially observed CTMC. Specifically, the simplest case occurs when the state of the CTMC is known at time 0 and at time t , while its behavior throughout the interval $(0, t)$ remains unknown. This implies that an object of major importance is the finite-time transition probability of starting at a time, say 0, on state i and being on state j at a later time, say t , that is:

$$P_{ij}(t) := \mathbb{P}(Y(t) = j \mid Y(0) = i). \quad (3)$$

Collecting all such values in a matrix whose rows represent the starting states and columns the ending states, we obtain the *finite-time transition probability matrix* $\mathbf{P}(t) = (P_{ij}(t))_{ij}$. If we assume the identity matrix \mathbf{I} as the initial condition of the system, that is the system is in its current state without any transitions at time $t = 0$, then it is easy to derive a closed-form formula for $\mathbf{P}(t)$ based on the infinitesimal rate matrix \mathbf{Q} :

$$\mathbf{P}(t) = e^{t\mathbf{Q}}, \quad (4)$$

where the matrix exponential is defined as follows:

$$e^{t\mathbf{Q}} := \sum_{i=0}^{\infty} \frac{(t\mathbf{Q})^i}{i!}. \quad (5)$$

Now we consider three cases where the data are only *partially observed*. We begin by assuming that we observe the data sequentially. Within this framework, we distinguish when the sampling times are known and when they are not. Then,

we briefly introduce the more general case where observations are not assumed to be sequential.

Observed sequential times The simplest partially observed scenario arises when the sequence of observations includes both the states and the corresponding sampling times (\mathbf{y}, \mathbf{t}) , but there is no guarantee that all the jumps of the CTMC are observed.

Then, we can write the joint distribution of (\mathbf{y}, \mathbf{t}) using the Markov property and the finite transition probabilities:

$$p(\mathbf{y}, \mathbf{t} | \mathbf{Q}) = \pi^*(y_1) \prod_{i=2}^N P_{y_{i-1}, y_i}(t_i). \quad (6)$$

With the exception of specific, mostly low-dimensional cases, such as the Jukes-Cantor (JK) substitution model (Jukes and Cantor, 1969) for DNA mutations, the values $P_{y_{i-1}, y_i}(t_i)$ are generally not available in closed-form. However, they can be computed by evaluating the matrix exponential for the specified time interval, which requires a computational effort of cubic-order ($\mathcal{O}(K^3)$).

Unobserved sequential times Suppose instead that the realizations in the vector \mathbf{y} are sequentially observed, but the observation times are unknown. From formula 4 it is clear that the waiting times and the infinitesimal rate matrix are jointly identifiable only up to a multiplicative factor. A candidate solution is to constrain the structure of \mathbf{Q} and define a new time scale dependent on the infinitesimal rate matrix.

To achieve this, let $\boldsymbol{\pi} = (\pi_1, \dots, \pi_K)$ be a probability mass vector on the K states in \mathbf{S} which represents the *a priori* state frequencies; $\boldsymbol{\pi}$ can represent \mathbf{Q} 's stationary distribution ($\boldsymbol{\pi} = \boldsymbol{\pi}^*$), but this need not be the case. Let $N_{\mathbf{Q}}(t)$ count the (random) number of jumps during the period $[0, t]$ with respect to the probability vector $\boldsymbol{\pi}$. It

can be shown that its expected value is equal to:

$$\mathbb{E}[N_{\mathbf{Q}}(t)] = t \sum_{i \in \mathbf{S}} \pi_i q_i, \quad (7)$$

recalling that $q_i = \sum_{j \neq i} q_{ij}$. A way to ensure this expected value depends only on time is to divide each element of the rate matrix \mathbf{Q} by a *normalizing constant* ψ equal to:

$$\psi = \mathbb{E}[N_{\mathbf{Q}}(1)] = \sum_{i \in \mathbf{S}} \pi_i q_i = \sum_{i \neq j} \pi_i q_{ij}. \quad (8)$$

Therefore, defining the matrix $\mathbf{\Lambda} = (\lambda_{ij})_{ij}$ as the normalized version of \mathbf{Q} , that is

$$\lambda_{ij} = \frac{1}{\psi} q_{ij} \quad \text{for every } i, j \in \{1, 2, \dots, K\}, \quad (9)$$

we have created a new CTMC where the expected number of jumps during a period $[0, t]$ is equal to the time:

$$\mathbb{E}[N_{\mathbf{\Lambda}}(t)] = t. \quad (10)$$

Using the normalized matrix constrains the rate values to satisfy Condition 10, solving the identifiability problem. Indeed, suppose we respectively multiply and divide the matrix $\mathbf{\Lambda}$ and time by a scale factor, then the scale factor disappears in the normalization step, implying that after the transformation, the normalized rate matrix is unchanged, while the time variable has changed.

This approach suggests that we can, and should, reinterpret time in terms of the expected number of jumps of the CTMC. For example, a unit time length is equal to the time necessary for the normalized CTMC to experience on average one jump ($\mathbb{E}[N_{\mathbf{\Lambda}}(1)] = 1$ by construction). In the phylogenetic literature, a field that heavily

relies on CTMCs, this time scale is often referred to as the “evolutionary time” scale, as opposed to the natural time scale. It provides a standardized way to compare processes that may evolve at different speeds.

Assigning a prior $p(\mathbf{t})$ to the times, the likelihood of the observed data conditional on the rate matrix is:

$$p(\mathbf{y} | \mathbf{Q}) = \int_{\mathbf{t} \in \mathbb{R}_+^N} p(\mathbf{y}, \mathbf{t} | \mathbf{Q}) p(\mathbf{t}) d\mathbf{t}, \quad (11)$$

where $p(\mathbf{y}, \mathbf{t} | \mathbf{Q})$ can be computed as in Equation 6.

CTMCs along an acyclic graph In a more general framework, a CTMC evolves along an acyclic and connected graph $\tau = (V, E)$ where V is the set of nodes and $E \subseteq V \times V$ is the set of edges. The value of the CTMC is then observed on some subset of nodes. Therefore, the likelihood $p(\mathbf{y} | \mathbf{Q})$ will have to be written accounting for the conditional independence structure that the graph induces. The case where the observations are sequential falls within this framework, assuming that the nodes are located along a line. Section 4 will develop in more detail the case where the graph is tree-shaped and the observations lie at the tree tips.

2.3 Prior on the infinitesimal rate matrix

Infinitesimal rate matrix parametrization The non-negativity constraints on the non-diagonal elements of the rate matrix \mathbf{Q} , if directly modeled, prevent the use of convenient prior distributions defined on the real line and complicate the use of gradient-based samplers. As is customary, we introduce a vector of auxiliary parameters $\boldsymbol{\theta} = (\theta_1, \theta_2, \dots, \theta_K)$ and link them to the rates by a non-negative differentiable one-to-

one transformation $g(\cdot)$, such that:

$$q_{ij} = g(\theta_{ij}). \quad (12)$$

For example, in this work, we shall examine the case when $g(\theta) = e^\theta$. Besides, henceforth the infinitesimal rate matrix will be studied as a function of $\boldsymbol{\theta}$, that is $\mathbf{Q} = \mathbf{Q}(\boldsymbol{\theta})$.

Covariate-based inference Now, consider a single one-dimensional covariate $\mathbf{x} = (x_{ij})_{ij}$ that associates a value to each pair of states ij . For example, x_{ij} could be the physical distance between two geographical states i and j which could affect the transition rate q_{ij} between them. We can then use such covariate to inform a prior on the parameters $\boldsymbol{\theta}$.

Gaussian processes as a prior choice To relax the restrictive assumptions of the log-linear model employed in the previous literature (Pybus et al., 2012; Lemey et al., 2014; Zhao et al., 2016), we propose to model the relationship between the parameters and the covariate using a more flexible GP prior. This allows us to capture complex, nonlinear dependencies that a log-linear framework cannot adequately represent.

Background on Gaussian processes The GP prior is a powerful Bayesian nonparametric prior that defines a distribution over more generic functions. Beyond accommodating nonlinearities, the GP enables a principled way to model uncertainty, as it provides not only point estimates but also credible intervals for inferred relationships. The GP is parameterized by a mean and a covariance function. The covariate function, also known as the GP *kernel*, defines the dependencies between function values at different input points, controlling both the smoothness and variability of the inferred function. By specifying an appropriate kernel, we can encode prior beliefs about the

structure of the relationship, such as stationarity, periodicity, or varying degrees of smoothness. Common choices include the squared exponential kernel, which enforces smooth variations, and the Matérn kernel, which allows for more flexible roughness.

GP prior: one covariate In mathematical terms we write the transformed rates θ_{ij} as a random function of covariates on which we assign a GP prior as follows:

$$\theta_{ij} = f(x_{ij}) \quad \text{with} \quad f(\cdot) \sim \mathcal{GP}(\mathbf{0}, \mathbf{k}(\cdot, \cdot | \boldsymbol{\alpha})), \quad (13)$$

where f is distributed as a GP with zero mean and kernel $\mathbf{k}(\cdot, \cdot | \boldsymbol{\alpha})$ parametrized by the vector of hyperparameters $\boldsymbol{\alpha}$.

GP prior: more covariates If we consider a set of P covariates $(\mathbf{x}_1, \mathbf{x}_2, \dots, \mathbf{x}_P)$, then we can model the parameters θ_{ij} with an additive GP prior (Duvenaud et al., 2011), that is:

$$\theta_{ij} = \sum_{p=1}^P f_p(x_{p,ij}) \quad \text{with} \quad f_p(\cdot) \stackrel{\text{ind}}{\sim} \mathcal{GP}(\mathbf{0}, \mathbf{k}_p(\cdot, \cdot | \boldsymbol{\alpha}_p)), \quad (14)$$

where all f_p 's are independent and allowed to have different kernels $\mathbf{k}_p(\cdot, \cdot | \boldsymbol{\alpha}_p)$. This last expression can then be integrated out leveraging the independence of the f_p 's. Specifically, in vector form, we obtain:

$$\boldsymbol{\theta} \sim \mathcal{GP}(\mathbf{0}, \sum_{p=1}^P \mathbf{k}_p(\mathbf{x}_p, \mathbf{x}_p' | \boldsymbol{\alpha}_p)). \quad (15)$$

This framework can then be easily generalized to account for interactions between covariates (Duvenaud et al., 2011).

3 Methods II: Inference

Limits of traditional MCMC methods The infinitesimal rates q_{ij} are governed by complex dependencies, and their number grows quadratically with the number of states K . This creates a high-dimensional parameter space with strong correlations among parameters. As a result, traditional random-walk Markov Chain Monte Carlo (MCMC) methods often mix slowly, exhibit high autocorrelation, and converge poorly.

Hamiltonian Monte Carlo We adopt HMC (Duane et al., 1987), a gradient-based sampling method that is particularly well-suited for traversing high-dimensional and strongly correlated posterior distributions. By introducing auxiliary momentum variables and simulating Hamiltonian dynamics, HMC is able to propose distant, informed updates that preserve detailed balance while reducing random walk behavior (Neal, 2011). This improves exploration of the parameter space, accelerates mixing, and lowers autocorrelation compared to standard MCMC methods.

Challenges with HMC gradient computation Each HMC update requires repeated computation of the likelihood gradient. In *partially observed* CTMCs, the likelihood depends on matrix exponentials of the infinitesimal rates. Differentiating these matrix exponentials is computationally demanding, typically requiring at least $\mathcal{O}(K^3)$ operations per evaluation. Since the number of distinct rates scales quadratically with the number of states, the total gradient costs at least $\mathcal{O}(K^5)$ per iteration. For large state spaces, this makes a naïve implementation of HMC infeasible.

HMC with surrogate trajectories Li et al. (2019) demonstrate that replacing the exact gradient of the log-posterior with an approximation thereof preserves the essential properties of HMC—such as reversibility and volume preservation—and that the ap-

plication of a Metropolis–Hastings correction step ensures the exact posterior remains the stationary distribution of the Markov chain. Building on this insight, we adopt the scalable approximation to the matrix exponential derivative proposed by [Magee et al. \(2024\)](#), reducing the computational complexity of the log posterior gradient evaluation by three orders of magnitude, making it quadratic in the number of states K with respect to all rate parameters simultaneously. In the next section, we shall provide closed-form expressions for the likelihood gradient, present the aforementioned approximation, and highlight its crucial role.

3.1 Likelihood's gradient computations

The difficulty of computing the likelihood gradient with respect to the transformed (un-normalized) rates $\theta_{ij} = g^{-1}(q_{ij})$ varies depending on the sampling scenario. For fully observed CTMCs, the gradient is straightforward from Equation 2, so it is omitted here. In contrast, for partially observed CTMCs, $p(\mathbf{y})$ involves multiple matrix exponentials that must be differentiated. Section 3.1.1 reviews a benchmark method for computing these exact gradients and shows that its cost quickly becomes prohibitive as the state space grows. Section 3.1.2 then demonstrates how adopting an approximation of those gradients is crucial in reducing that cost and in making inference feasible, while Section 3.1.3 compares our approach with exact gradient computations based on automatic differentiation. We also apply the approximation directly to sequentially observed CTMCs with known sampling times, where the finite-time transition probability matrices do not depend on the normalizing constant. Conversely, for the other partially observed processes, Section 3.1.4 provides an explicit derivation of the gradient of $p(\mathbf{y})$ with respect to the transformed un-normalized rates accounting for the presence of the normalization constant.

3.1.1 Gradient of the matrix exponential: Costly exact method

[Najfeld and Havel \(1995\)](#) review several strategies for computing the gradient of a matrix exponential. Among these, one of the most popular and straightforward approaches relies on an augmentation method. Specifically, to compute the gradient of $e^{t\mathbf{\Lambda}}$ with respect to λ_{ij} , we construct the block matrix

$$\mathbf{B} = \begin{bmatrix} \mathbf{\Lambda} & \mathbf{E}_{ij} \\ \mathbf{0} & \mathbf{\Lambda} \end{bmatrix}, \quad (16)$$

where \mathbf{E}_{ij} denotes a matrix of zeros except for a single one in position ij . Exponentiating \mathbf{B} and extracting its upper-right block yields the Fréchet derivative of $e^{t\mathbf{\Lambda}}$ in the direction of \mathbf{E}_{ij} —that is, the gradient with respect to λ_{ij} . The computational cost of this exponentiation scales cubically with twice the dimension of $\mathbf{\Lambda}$. Alternative analytical methods exhibit comparable asymptotic complexity, differing primarily by constant factors. For instance, [Kalbfleisch and Lawless \(1985\)](#) derive a closed-form expression for the gradient when $\mathbf{\Lambda}$ is diagonalizable, which remains cubic in the number of states. However, in our setting, diagonalizability constitutes an overly restrictive assumption. To conclude, since gradients must be evaluated for every non-diagonal element of $\mathbf{\Lambda}$, the overall computational complexity of any such method is $\mathcal{O}(K^5)$, rendering these approaches computationally prohibitive even for moderate K .

3.1.2 Gradient of the matrix exponential: Scalable approximation

A scalable approximation An alternative way to express the *exact* gradient of a matrix exponential is through the following series ([Najfeld and Havel, 1995](#)):

$$\frac{\partial}{\partial \lambda_{ij}} e^{t\mathbf{\Lambda}} = e^{t\mathbf{\Lambda}} \sum_{k=0}^{\infty} \frac{t^{k+1}}{(k+1)!} \{\mathbf{E}_{ij}, \mathbf{\Lambda}^k\}, \quad (17)$$

where \mathbf{E}_{ij} is a matrix with zero at all entries but at ij where it is equal to one. Moreover, $\{\mathbf{E}_{ij}, \mathbf{\Lambda}^k\}$ is defined recursively as $\{\mathbf{E}_{ij}, \mathbf{\Lambda}^0\} = \mathbf{E}_{ij}$ and $\{\mathbf{E}_{ij}, \mathbf{\Lambda}^k\} = [\{\mathbf{E}_{ij}, \mathbf{\Lambda}^{k-1}\}, \mathbf{\Lambda}]$, where $[\cdot, \cdot]$ is the matrix commutator. The operational implementation of Equation 17 requires truncating the infinite series to a finite number of terms. Fortunately, [Didier et al. \(2024\)](#) demonstrate that retaining only the first term of the series already provides a remarkably accurate first-order approximation:

$$\frac{\partial e^{t\mathbf{\Lambda}}}{\partial \lambda_{ij}} \approx t e^{t\mathbf{\Lambda}} \mathbf{E}_{ij}. \quad (18)$$

This choice dramatically decreases the computational complexity. Although this approximation still depends on the matrix exponential $e^{t\mathbf{\Lambda}}$, this quantity is already required for likelihood evaluation and can therefore be precomputed once and cached. Furthermore, while the multiplication of two matrices of same dimensions ordinarily scales cubically, the sparsity of \mathbf{E}_{ij} ensures that the product in Equation 18 is highly efficient: it produces a matrix that is zero everywhere except for its j -th column that is a copy of the i -th column of $e^{t\mathbf{\Lambda}}$. Since each element of this non-zero column has to be multiplied by t , the output sparse matrix can be generated in $\mathcal{O}(K)$. Repeating this computation for each entry of the rate matrix entails a total number of operations of order $\mathcal{O}(K^3)$ versus the $\mathcal{O}(K^5)$ for the exact approach.

Application to CTMC likelihood's gradients In the context of the CTMC likelihood's gradients $\frac{\partial p(\mathbf{y})}{\partial \lambda_{ij}}$, we can further leverage both the structure of $p(\mathbf{y})$ and the sparsity of \mathbf{E}_{ij} to reduce the number of operations below cubic. In the next two paragraphs we consider the simpler scenario with a single CTMC observed sequentially with known sampling times as in Equation 6, while Section 4 extends the same result to the case where the CTMC evolves along a tree-like graph.

When observations are *sequential*, the likelihood can be written as a product of

the finite-time transition probabilities that the CTMC starting at a state y_{u-1} ends up on state y_u after time t_u , that is, $P_{y_{u-1},y_u}(t_u)$ for each observation u . We can then rewrite each of those factors as an inner product as follows:

$$P_{y_{u-1},y_u}(t_u) = \mathbf{u}'_{u-1} \mathbf{P}(t_u) \mathbf{u}_u = \mathbf{u}'_{u-1} e^{t_u \mathbf{\Lambda}} \mathbf{u}_u, \quad (19)$$

where \mathbf{u}_u is a K -dimensional vector with all zero entries but for the one corresponding to the value of y_u . The gradient of $P_{y_{u-1},y_u}(t_u)$ with respect to one rate using the aforementioned approximation is then equal to:

$$\frac{\partial P_{y_{u-1},y_u}(t_u)}{\partial \lambda_{ij}} = t_u \mathbf{u}'_{u-1} e^{t_u \mathbf{\Lambda}} \mathbf{E}_{ij} \mathbf{u}_u. \quad (20)$$

Assuming that the matrix exponential was pre-computed and cached when the likelihood was evaluated, the expression above can be calculated in $\mathcal{O}(1)$ time since it either outputs one entry of the matrix exponential or 0. To conclude, if we need to compute the gradient in Equation 20 for each of the $K^2 - K$ non-diagonal entries of $\mathbf{\Lambda}$ and for each of $N - 1$ pair of consecutive observations, we achieve a total computational complexity of $\mathcal{O}(NK^2)$. Therefore, operationally, we have further reduced the complexity from cubic to quadratic in the number of states K .

3.1.3 A Comparison with automatic differentiation

Automatic differentiation (AD) methods have become a cornerstone of modern scientific computing, particularly in fields like machine learning and optimization. By providing efficient and exact ways to compute derivatives, they have enabled the development of complex models that were previously intractable (Margossian, 2019). In general, AD algorithms are divided into two main modes: forward mode and reverse mode. Forward-mode AD is most efficient when the function of interest depends on

a small number of inputs but produces many outputs, whereas reverse-mode AD is preferable when there are many input variables and few output quantities (Baydin et al., 2018). Given our framework’s structure—with many input variables (the rates) and a single scalar output (the joint distribution)—reverse-mode AD constitutes the natural choice for gradient evaluation. This method requires a forward pass to compute the function value, which scales as $\mathcal{O}(K^3)$, followed by a single backward pass to obtain all parameter gradients simultaneously. The backward pass requires computing the *adjoint* of the derivative of the matrix exponential, an operation of comparable complexity, also $\mathcal{O}(K^3)$.

Following the same reasoning as in the previous section, within the context of CTMCs, evaluating the likelihood gradient requires at least $N - 1$ adjoint computations, resulting in an overall computational complexity of $\mathcal{O}(NK^3)$. Although this represents a substantial improvement over performing a full sequence of exact gradient evaluations for each individual rate parameter, it remains an order of magnitude more expensive than directly applying the proposed approximate gradient. The gap in efficiency becomes even more pronounced when considering the large K -invariant constant factor embedded in the $\mathcal{O}(NK^3)$ cost. Specifically, computing the adjoint using the exact gradient from Equation 16 requires the evaluation of a matrix exponential of dimension $2K \times 2K$, whose cubic scaling implies a computational burden proportional to $(2K)^3 = 8K^3$. Moreover, even the most efficient algorithms for computing a matrix exponential require work equivalent to about 29 matrix-matrix multiplications (Najfeld and Havel, 1995).

In contrast, the proposed approximate gradient formulation completely avoids such heavy operations. It relies solely on matrix-vector products, not only reducing asymptotic complexity but also yielding a substantial reduction in expected runtime due to improved memory locality and reduced numerical overhead.

3.1.4 Gradient with respect to the auxiliary parameters θ_{ij}

In the context of partially observed CTMCs where a normalization constant is necessary for identifiability reasons, the likelihood $p(\mathbf{y})$ depends directly only on the normalized rates λ_{ij} . Therefore, differentiating $p(\mathbf{y})$ with respect to a transformed un-normalized rate $\theta_{ij} = g^{-1}(q_{ij})$ needs to account for its effects on each of the normalized rates (and so on the normalization constant). We now derive this gradient and evaluate it when the link function g is exponential.

Since $p(\mathbf{y})$ depends on θ_{ij} (and so on q_{ij}) through the normalized rates λ_{ij} , we need to apply the chain rule on $p(\mathbf{y})$, separating the effect of θ_{ij} on each λ_{ij} , that is:

$$\begin{aligned} \frac{\partial p(\mathbf{y})}{\partial \theta_{ij}} &= \sum_{uv} \frac{\partial p(\mathbf{y})}{\partial \lambda_{uv}} \frac{\partial \lambda_{uv}}{\partial \theta_{ij}} = \sum_{uv} \frac{\partial p(\mathbf{y})}{\partial \lambda_{uv}} \left(\frac{1}{\psi} \frac{\partial q_{uv}}{\partial \theta_{ij}} - q_{uv} \frac{1}{\psi^2} \frac{\partial \psi}{\partial \theta_{ij}} \right) \\ &= \sum_{uv} \frac{\partial p(\mathbf{y})}{\partial \lambda_{uv}} \frac{1}{\psi} \frac{\partial q_{uv}}{\partial \theta_{ij}} - \sum_{uv} \frac{\partial p(\mathbf{y})}{\partial \lambda_{uv}} q_{uv} \frac{1}{\psi^2} \frac{\partial \psi}{\partial \theta_{ij}}. \end{aligned} \quad (21)$$

Noticing that $\frac{\partial q_{uv}}{\partial \theta_{ij}} = 0$ for all $uv \neq ij$ or ii , we can re-write the first summation in Equation 21 as:

$$\sum_{uv} \frac{\partial p(\mathbf{y})}{\partial \lambda_{uv}} \frac{1}{\psi} \frac{\partial q_{uv}}{\partial \theta_{ij}} = \left(\frac{\partial p(\mathbf{y})}{\partial \lambda_{ij}} - \frac{\partial p(\mathbf{y})}{\partial \lambda_{ii}} \right) \frac{1}{\psi} \frac{\partial q_{ij}}{\partial \theta_{ij}} = \Delta(\mathbf{y})_{ij} \frac{1}{\psi} \frac{\partial q_{ij}}{\partial \theta_{ij}} \quad (22)$$

where $\Delta(\mathbf{y})_{ij} := \left(\frac{\partial p(\mathbf{y})}{\partial \lambda_{ij}} - \frac{\partial p(\mathbf{y})}{\partial \lambda_{ii}} \right)$ is the difference between the partial derivative with respect to a non-diagonal element and its corresponding diagonal element's. We can then plug in Equation 22 into Equation 21 and input the exponential link function $q_{ij} = e^{\theta_{ij}}$ such that:

$$\frac{\partial p(\mathbf{y})}{\partial \theta_{ij}} = \left[\Delta(\mathbf{y})_{ij} - \left(\sum_{uv} \frac{\partial p(\mathbf{y})}{\partial \lambda_{uv}} \lambda_{uv} \right) \pi_u \right] \lambda_{ij}. \quad (23)$$

Now, notice that these expressions only depend on the distribution vector $\boldsymbol{\pi}$, the nor-

malized rates λ_{ij} , and the gradient of $p(\mathbf{y})$ with respect to each normalized rate. We can therefore evaluate it directly plugging in the matrix exponential approximations that we derived above.

4 Adaptation to phylogeographic inference

Phylogeography is an area of study that heavily relies on CTMCs. One of the distinguishing characteristics of this field is that data are assumed to enjoy a tree-shaped dependency structure. This complicates the computation of the likelihood, motivating the use of efficient sampling techniques even more.

In the following section, we review the fundamental building blocks of Bayesian phylogenetics and hence phylogeography. We begin by defining a tree and then describe how discrete data are assumed to be generated along it. Then, we compute the likelihood and demonstrate how the approximation introduced in the previous section plays a crucial role in significantly reducing the computational burden of the gradient evaluations. Finally, we apply our methods to synthetic and real data examples.

4.1 Introduction to Bayesian phylogenetics

The phylogeny A **tree** or **phylogeny** \mathcal{F} is a pair $\langle \tau, \mathcal{B} \rangle$ where:

- $\tau = (V, E)$ is an acyclic and connected graph, with V being the set of nodes and $E \subseteq V \times V$ being the set of edges. We shall refer to τ as the *topology* of the tree and to the edges as *branches*. The number of edges that are connected to a specific node is named *degree* of the node.
- \mathcal{B} is the set of *branch lengths*, a measure of the distance between two nodes directly connected by one edge.

In this work, we assume there is a (possibly unknown) rooted phylogeny \mathcal{F} with N tips

(the “leaves” of the tree), called *taxa*, and $N - 1$ internal nodes. Since the topology is acyclic, the N tips have degree 1, the $N - 2$ internal nodes have degree 3, while one node, the root, has degree 2. Considering two nodes u_1 and u_2 both connected with an edge to a third node v closer to the root than both, we say that v is the parent node and write $pa(u_1) = v$ and $pa(u_2) = v$; on the other hand, u_1 and u_2 are said siblings and we write, for example, $sibl(u_1) = u_2$. By convention, we refer to the branch connecting a parent node v to its child node u by the name of the child node, u , and denote its length by t_u .

The data generating process The data-generating process is modeled as a CTMC that originates at the root and evolves along the tree in accordance with its conditional independence structure. We denote the realized values of the CTMC at node i with y_i . Such realized values are assumed to be unknown for the internal nodes, while they are observed at the tips of the tree. We refer to such observed values with the vector $\mathbf{y} = (y_1, y_2, \dots, y_N)$, where $1, 2, \dots, N$ index the N tips of the tree.

Phylogenetics inference The parameters of interest within the inferential process are usually the phylogeny \mathcal{F} and CTMC infinitesimal rates ($\mathbf{Q} = (q_{ij})$), or the quantities on which these rates depend ($\boldsymbol{\theta}$). If we assign a prior $p(\mathcal{F})$ to the tree and a prior $p(\boldsymbol{\theta})$ to the CTMC parameters, then the posterior distribution can be written as:

$$p(\boldsymbol{\theta}, \mathcal{F} | \mathbf{y}) \propto p(\mathbf{y} | \mathcal{F}, \mathbf{Q}(\boldsymbol{\theta})) p(\boldsymbol{\theta}) p(\mathcal{F}), \quad (24)$$

where $p(\mathbf{y} | \mathcal{F}, \mathbf{Q}(\boldsymbol{\theta}))$ is usually referred to as the *tree data likelihood*. Computing the tree data likelihood implies integrating out all the values of the unobserved nodes and will be the subject of the next section.

4.2 Computing the tree data likelihood

Let $\mathbf{y} = (y_1, \dots, y_N)$ be the data observed at the tips of an N -taxa tree and v be an internal node. Denote by $y_{[v]}$ the subset of \mathbf{y} collecting all the descendants of v , while $y_{[v]}$ collects the non-descendants in \mathbf{y} . The joint distribution of the observed tip values, known as the *tree data likelihood*, is given by $p(\mathbf{y} | \mathcal{F}, \mathbf{Q})$. A convenient method to compute this likelihood is shown in the following expression, where we omit the explicit dependence on the parameters for simplicity:

$$\begin{aligned}
 p(y_1, \dots, y_N) &= \mathbb{E} [p(y_1, \dots, y_N | y_v)] && \text{by the law of iterated expectations} \\
 &= \mathbb{E} [p(y_{[v]} | y_v) p(y_{[v]} | y_v)] && \text{by conditional independence} \\
 &= \sum_{y_v \in \mathbf{S}} p(y_v) p(y_{[v]} | y_v) p(y_{[v]} | y_v) \\
 &= \sum_{y_v \in \mathbf{S}} p(y_{[v]}, y_v) p(y_{[v]} | y_v) \\
 &= \mathbf{p}_v' \mathbf{q}_v,
 \end{aligned} \tag{25}$$

where \mathbf{p}_v is the vector of joint distributions of the descendants taxa of node v *conditioned* on each of the values that y_v can take, i.e., s_1, s_2, \dots, s_K . In contrast, \mathbf{q}_v is the joint distribution of the non-descendants of node v *joint* with each of the possible values that y_v can take. In phylogenetics, \mathbf{q}_v is named a *pre-order partial likelihood* vector, while \mathbf{p}_v is referred to as a *post-order partial likelihood* vector.

4.2.1 Iterative algorithm for the pre- and post-order partial likelihood computations

Consider three nodes where v is the parent, and u_1 and u_2 are the two children. The post-order partial likelihood vector \mathbf{p}_v can be computed using a pruning algorithm

from the tips to the root (post-order traversal) using:

$$\mathbf{p}_v = \mathbf{P}(t_{u_1}) \mathbf{p}_{u_1} \circ \mathbf{P}(t_{u_2}) \mathbf{p}_{u_2}, \quad (26)$$

where \circ represents the *Hadamard* or element-wise product. In other words, we take the post-order partial likelihood vectors of the two children nodes, and we “move” them up the branch pre-multiplying them by the finite transition matrix; then, since we want both independent conditions on the children nodes to hold, we multiply them together. On the other hand, the pre-order partial likelihood vector \mathbf{q}_{u_1} is derived in a root-to-tips tree exploration process (a pre-order-traversal) following the relation:

$$\mathbf{q}_{u_1} = \mathbf{P}(u_1)' (\mathbf{q}_v \circ \mathbf{P}(u_2) \mathbf{p}_{u_2}). \quad (27)$$

Notice that when the chosen reference node is a tip, the post-order partial likelihood is a Dirac measure. In particular, it assigns 1 to the observed state and zero to all other possible states. Besides, the pre-order partial likelihood at the root node must be fixed *a priori*; we denote it by $\boldsymbol{\pi}_{\text{root}}$. Finally, notice that applying the formulas above iteratively means going through each node just once, that is the computation of the tree data likelihood is linear in the number of observed tips (Felsenstein, 1981).

4.3 HMC with an approximate gradient

In the current work, we employ a Metropolis-within-Gibbs MCMC framework to sample from the full posterior distribution in Equation 24 (Metropolis et al., 1953; Geman and Geman, 1984). Within this framework, we partition the parameters into two blocks: the CTMC parameters, $\boldsymbol{\theta}$, and a second block containing all other parameters. While we adopt standard random-walk kernels to propose the second block of parameters

following the rich and established literature in Bayesian phylogenetics (Hassler et al., 2023), we use an HMC sampler with surrogate trajectories (Duane et al., 1987; Li et al., 2019) for the CTMC parameters as detailed in Section 3.

To make the HMC operational, we proceed by computing the explicit form for the derivative of the tree data likelihood function using the aforementioned approximation of the matrix exponential gradient. As we showed for the case of a sequentially observed CTMC with known sampling times (Section 3.1.2), also for a tree-based likelihood we can exploit the sparsity of the matrix \mathbf{E}_{ij} in the gradient approximation from Equation 18 to further reduce the computational complexity and derive an easily operationalizable formula. Specifically, based on the calculations shown in Appendix 6.1, the gradient of the tree data likelihood with respect to the normalized rates can be written as follows (Magee et al., 2024):

$$\frac{\partial p(\mathbf{y})}{\partial \lambda_{ij}} = \sum_{u=1}^{2N-2} \mathbf{p}'_u \left[\frac{\partial e^{t_u \mathbf{\Lambda}}}{\partial \lambda_{ij}} \right]' \tilde{\mathbf{q}}_{\text{pa}(u)} + \mathbf{p}'_{2N-1} \frac{\partial}{\partial \lambda_{ij}} \boldsymbol{\pi}_{\text{root}}, \quad (28)$$

where $\tilde{\mathbf{q}}_{\text{pa}(u)} := [\mathbf{q}_{\text{pa}(u)} \circ \mathbf{P}(t_{\text{sibl}(u)}) \mathbf{p}_{\text{sibl}(u)}]$. Substituting $\frac{\partial e^{t_u \mathbf{\Lambda}}}{\partial \lambda_{ij}}$ by the approximation presented in Equation 18, we can re-write the first summation on the right hand side of Equation 28 in a substantially simpler form:

$$\begin{aligned} \sum_{u=1}^{2N-2} \mathbf{p}'_u \left[\frac{\partial e^{t_u \mathbf{\Lambda}}}{\partial \lambda_{ij}} \right]' \tilde{\mathbf{q}}_{\text{pa}(u)} &= \sum_{u=1}^{2N-2} \mathbf{p}'_u [t_u e^{t_u \mathbf{\Lambda}} \mathbf{E}_{ij}]' \tilde{\mathbf{q}}_{\text{pa}(u)} \\ &= \sum_{u=1}^{2N-2} t_u \mathbf{p}'_u \mathbf{E}'_{ij} [e^{t_u \mathbf{\Lambda}}]' \tilde{\mathbf{q}}_{\text{pa}(u)} \\ &= \sum_{u=1}^{2N-2} t_u \mathbf{p}'_u \mathbf{E}'_{ij} \mathbf{q}_u \\ &= \sum_{u=1}^{2N-2} t_u p_{uj} q_{ui}, \end{aligned} \quad (29)$$

where p_{uj} and q_{ui} are the components respectively of \mathbf{p}_u and \mathbf{q}_u , and we apply Equation 27 in the third line. The approximation reduces the computational complexity for computing $\frac{\partial p(\mathbf{y})}{\partial \lambda_{ij}}$ from $\mathcal{O}(NK^3)$ using the traditional matrix exponential gradient computation (Kalbfleisch and Lawless, 1985) to just $\mathcal{O}(N)$, where N stems from the summation in Equation 29. Since we have to repeat these calculations for each entry of the infinitesimal matrix, the total computational complexity of our proposed method becomes of order $\mathcal{O}(NK^2)$ versus $\mathcal{O}(NK^5)$ for the exact method.

4.4 Results

In this section, we present a simulation study and two real-world examples that illustrate the proposed methods. Moreover, we estimate empirically the scalability of the gradient approximation as the state-space dimension increases. All the following analyses are run using the popular and open-source software BEAST X (Baele et al., 2025b) supported by the high-performance computing environment BEAGLE (Ayres et al., 2019). The simulated data are generated using π BUSS (Bielejec et al., 2014). The code and data to reproduce our analysis can be found at the publicly available GitHub repository <https://github.com/suchard-group/NonParametricModelingofCTMCs>.

4.4.1 Simulation

To assess the performance of the proposed methods for parameter estimation, we conduct a simulation study. Based on Faria et al. (2011), we begin by considering a CTMC describing the transmission process of the rabies virus infecting 17 host bat species. Each pair of species is associated with their genetic distances.

For simulation purposes, we set the log-rates of the CTMC equal to a quadratic function of those genetic distances as shown in Figure 1 (dashed line). Next, we select a phylogenetic tree sampled from the posterior distribution given aligned genomic

sequences obtained in [Faria et al. \(2011\)](#), containing 372 tips and spanning an evolutionary history of approximately 270 years. Subsequently, we simulate a single alignment (one observation per tip) by evolving the CTMC along the tree branches, starting from the root. The evolutionary rate, representing the average “speed” of evolution, is fixed at 2% per year. This corresponds to an expected total of roughly five transitions along the path from the root to the most recent tip.

To analyze the simulated data, we employ a GP prior on the log-rates, using a squared exponential kernel with the host-species genetic distances as a covariate. We place independent exponential priors with rate 1 to the kernel hyperparameters (the marginal scale and the length-scale). As shown in [Figure 1](#) (red line), the method recovers the underlying nonlinear log-rate function. As a comparison, we also run the analysis using a log-linear model (LL, blue line). Quantitatively, across posterior draws the GP achieves a median root mean square error (RMSE) of 0.170 (95% highest posterior density interval (HPDI) 0.039–0.311), versus 0.487 (95% HPDI 0.404–0.589) for the LL model—a $\approx 65\%$ reduction ($LL \approx 2.9\times$ larger), indicating superior accuracy. Moreover, pointwise 95% HPDI coverage of the true log-rate function is 100% for the GP and 28.68% for the log-linear model, with average HPDI widths of 0.63 and 0.39, respectively; thus, the GP bands are slightly wider, as expected, but substantially better calibrated.

We also used the simulation study to compare the efficiency of the approximate gradient against exact alternatives. For simplicity, the GP hyperparameters were fixed at their posterior medians estimated above, so that the only random quantities are the log-rates. All computations were performed on a Mac with an Apple M1 Pro processor, 8-core CPU, and 16 GB of RAM.

A two-step iteration of HMC using the exact gradient based on [Equation 16](#) required roughly one minute, whereas a 100-step iteration with the approximate gradient

completed in less than a second. Convergence of the approximate method was achieved within one to two days, while the exact method failed to converge after a full week of computation—even under different combinations of HMC tuning parameters. This demonstrates that the computational efficiency gains of the approximate method outweigh the potential precision advantages of the exact gradient.

We have also tested our method against an exact gradient computed numerically using central differences. This approach requires two evaluations of the tree data likelihood for each log-rate with a computational cost of $\mathcal{O}(K^3 + NK^2)$, driven by a cubic-time eigendecomposition of the generator matrix and quadratic-time matrix–vector products for each branch. Therefore, computing the numerical gradient for all rates amounts to a total computational complexity of $\mathcal{O}(K^5 + NK^4)$, which is an order of magnitude improvement over the exact gradient from Equation 16 when N is large. A 10-step iteration of HMC using the central-difference numerical gradient takes an average of nine seconds. However, as with the exact method, this approach did not reach convergence after a week of computation, despite extensive tuning of HMC parameters.

We must note that updating the hyperparameters entails a high computational cost. Indeed, when the kernel is modified, the GP covariance matrix also changes, requiring operations with cubic-time complexity in its dimension (e.g., inversion or Cholesky decomposition). Since the Gaussian density must be evaluated for $K^2 - K$ elements, the overall computational complexity increases to $\mathcal{O}(K^6)$. Fortunately, the hyperparameters are low-dimensional, and it therefore suffices to update them only occasionally. A profiling analysis of our simulation indicates that this cost is negligible when $K = 17$. However, as the state space grows, this cost may become non-trivial. Still, it should be compared with the cost of the likelihood and gradient evaluations, which both scale with the number of states and the number of observations—the latter

of which must also increase to provide sufficient information for all analyzed states.

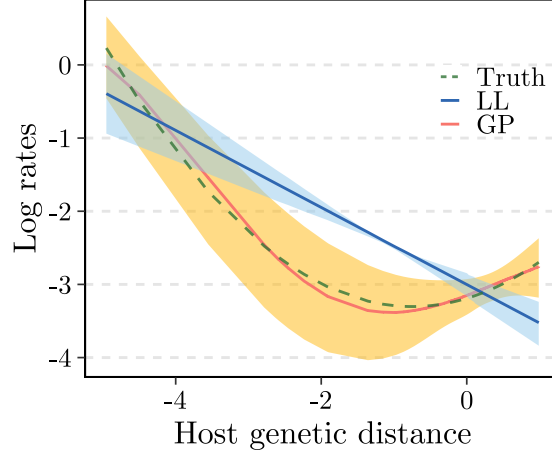


FIGURE 1: SIMULATION STUDY

Note: The figure shows a performance comparison between the log-linear (LL) and Gaussian process (GP) models in recovering the CTMC log-rates in a simulated dataset. The dashed line represents the true log-rates, which were set as a quadratic function of the host genetic distances. The solid lines show the posterior median normalized log-rates inferred under the LL (blue) and the GP (red) models, while the shaded areas cover the 95% highest posterior density intervals (HPDIs).

Only slope uncertainty is depicted, as all values are normalized.

Finally, we compare the gradient evaluation times between the approximate and the numerical gradients as a function of the number of states K . As discussed above, we expect the time complexities of these evaluations to respectively be $\mathcal{O}(K^2)$ and $\mathcal{O}(K^5)$. We begin by defining K states $(1, 2, \dots, K)$ and by assigning to each pair thereof a covariate value equal to the negative $L1$ distance between their indices, i.e., $(2, 5)$ yields $x_{2,5} = -|2 - 5| = -3$. We then construct a CTMC by setting the log-rates as follows:

$$q_{ij} = \log(x_{ij} + \max_{kl}(|x_{kl}|) + 1), \quad (30)$$

where the additive constants ensure non-negativity. This implies that the closer two states (i, j) are, the higher their associated log-rates. Using this CTMC, we simulate one alignment over the same tree used in the previous simulation. For a logarithmically

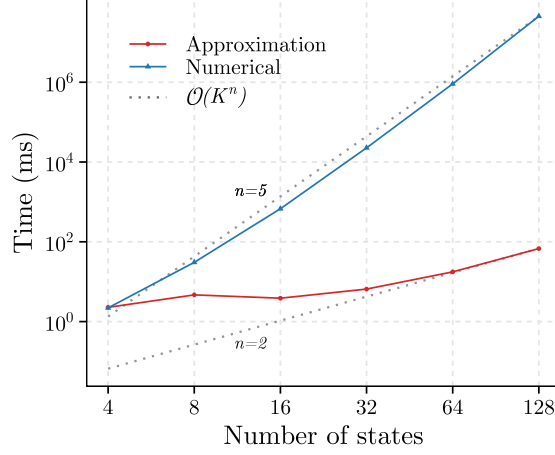


FIGURE 2: COMPUTATIONAL SPEED COMPARISON

Note: The figure shows a comparison of the average time (milliseconds, ms) per gradient evaluation as a function of the number of CTMC states between the approximate (red circles) and the exact numerical gradient (blue triangles). Dotted lines indicate theoretical scaling trends, $\mathcal{O}(K^2)$ for the approximate and $\mathcal{O}(K^5)$ for the numerical gradients, anchored at the estimated times for 128 states.

increasing sequence of states, $K = 4, 8, 16, 32, 64, 128$, we record the average computational time required per gradient evaluation. Figure 2 illustrates that the empirically observed times are consistent with the corresponding theoretical expectations for time complexity. In particular, we construct a *log-log* plot that juxtaposes the two empirical curves—one for the approximate gradient (red) and one for the numerical gradient (blue)—alongside two reference lines with slopes 2 and 5, respectively, which represent the theoretical scaling rates predicted for each method. The close alignment between the empirical trends and the reference slopes further corroborates the expected computational scaling behavior of the two gradient formulations.

4.4.2 Bat rabies viruses in North America

After validating our method on simulated data, we apply it to two real-world examples. We start by reproducing the analysis performed in [Faria et al. \(2013\)](#) of a dataset composed of 372 rabies virus samples collected from 17 species of infected bats in North

America between 1997 and 2006 ([Streicker et al., 2010](#)). This study reconstructs the evolutionary history of the rabies viruses based on the sequences of the nucleoprotein gene, the location of the samples, as well as the species each host bat belongs to. Moreover, the authors investigate the transmission dynamics between different bat species in order to identify potential facilitating factors. Using a log-linear model, they conclude that cross-species genetic distance influences transmission: the more two bat species are genetically different, the less likely a transmission event.

We revisit these data, relaxing the log-linear assumption. Specifically, we assign to the infinitesimal log-rates a GP prior with a squared exponential kernel using the host genetic distance as a covariate. Moreover, we specify two exponential priors with rates 1 and 2, respectively, for the kernel scale and length hyperparameters. To avoid overfitting, we also constrain the length parameter to be at least one. As [Figure 3a](#) highlights, our results support the hypothesis that the genetic distance has a log-linear effect on the infinitesimal rates. The relation between this covariate and the rabies virus evolutionary history can also be visualized from a comparison of the two trees shown in [Figure 4](#). On the left, the reader can see a viral tree that is produced according to the maximum credibility clade (MCC) criterion ([Baele et al., 2025a](#)). This method selects the single tree that best represents the most well-supported clades from the full distribution of sampled trees, where a clade can be defined as a subset of the complete tree including a common ancestor and all of its descendants. Branches are colored based on the bat species most likely to harbor the virus throughout their corresponding period. On the right, a dendrogram illustrates the hierarchical clustering of bat species based on cross-species genetic distances, with groupings determined by Ward’s method ([Ward Jr., 1963](#)), that is, by minimizing the within-cluster variance. It is apparent that the two trees have a symmetric color-induced structure, suggesting a tendency for infection events to occur more frequently across more closely related species.

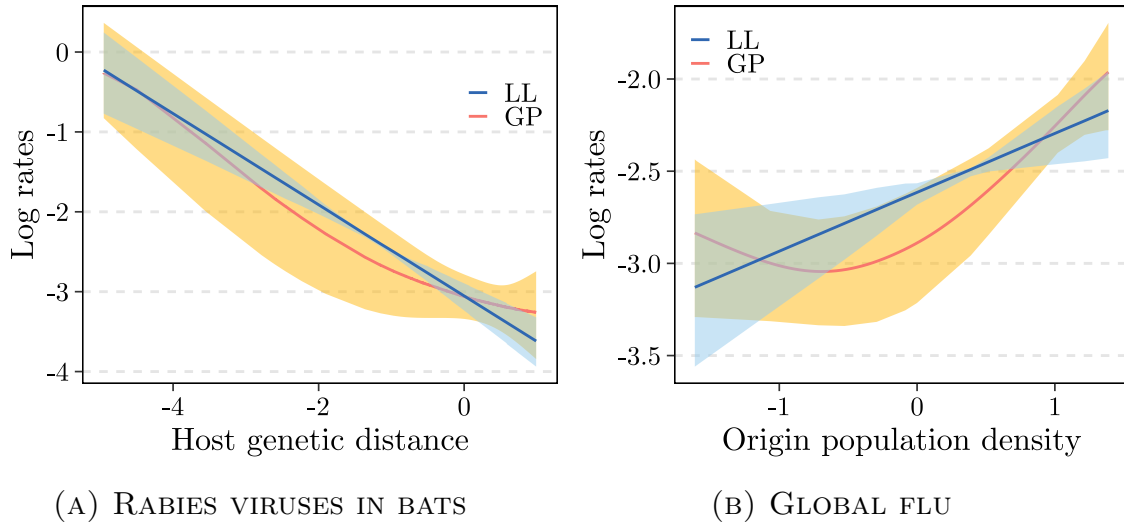


FIGURE 3: DATA EXAMPLES: LOG-RATES VS PREDICTORS

Note: These images illustrate the relationships between the log-rates and the predictors in two data sets. In particular, Figure 3a portrays the effect of the cross-species genetic distances in the rabies virus dataset, while Figure 3b focuses on the effect of the population density of the origin country in the transmission of the global flu. The solid lines represent the posterior median inferred log-rates under a log-linear (LL) and a Gaussian process-based (GP) models, while the shaded areas show the 95% HPDIs. Notice that only the uncertainty in the slope is depicted, since all values are normalized.

4.4.3 Global Influenza and human transportation

As a second example, we use data on the global spread of seasonal H3N2 influenza between 2002 to 2007. The data consists of hemagglutinin sequences and sample locations from 1,441 human-sampled viral isolates, and were originally analyzed by [Lemey et al. \(2014\)](#) to study the annual spread of the virus across 14 global air communities. The authors' original work used a log-linear model to guide the spatial dispersion process, leveraging covariates such as airplane seat numbers and origin country population densities.

Focusing on origin country population densities, we aim to relax the log-linear assumption by modeling the covariate effect using a GP. We adopt a squared-exponential kernel and assign two exponential priors with rates 1 and 2 respectively to the marginal scale and length-scale hyperparameters. Also, to avoid over-fitting, we constrained the

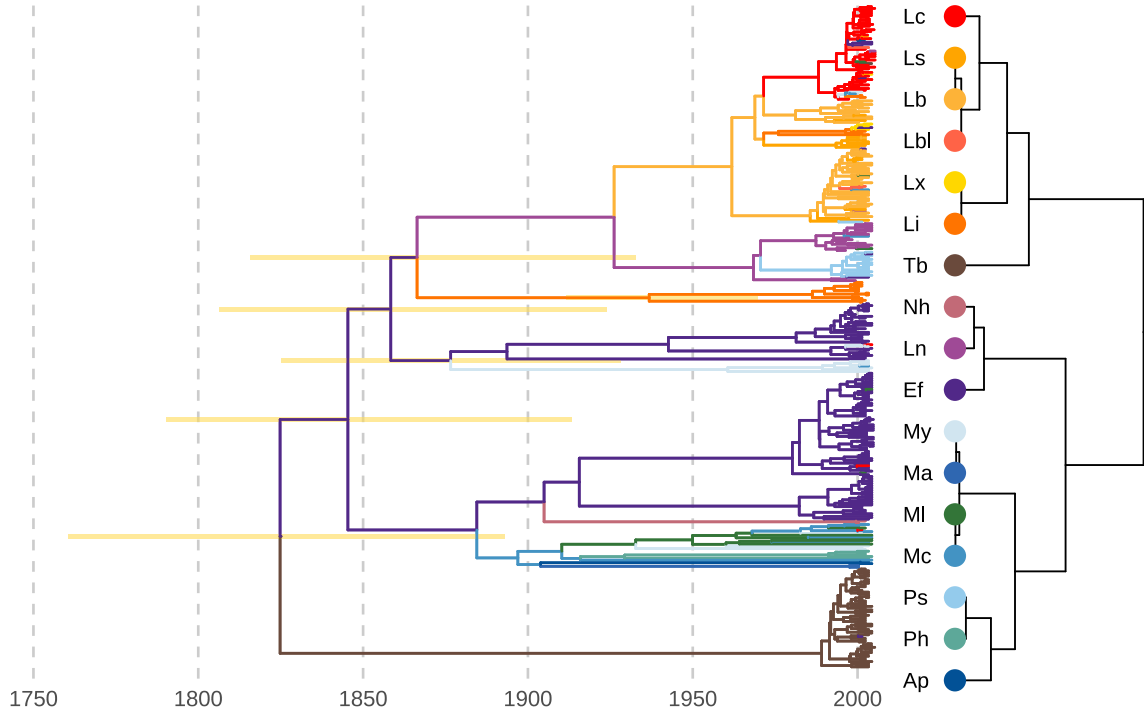


FIGURE 4: BAT RABIES DATA EXAMPLE

Note: On the left, the viral tree shows the evolution of the rabies virus in a population of bats in North America. The yellow rectangular bars represent the 95% HPDIs for the age of the corresponding node. The colors along each branch identify the most probable bat species hosting the rabies virus at that point in time. Besides, the tree on the right orders the bat species based on their genetic distance as outputted by Ward's hierarchical clustering algorithm (Ward Jr., 1963). Comparing the two trees it stands out the symmetry in the distribution of the colors (bats species), supporting the hypothesis that the rabies viruses tend to be transmitted more across genetically more similar bat species.

length parameter to be bigger than 1.

Figure 3b compares the inferred log-rates from both the log-linear and the GP models. The results suggest that the log-linear assumption is too restrictive, as it appears to overestimate the effect of low population densities while underestimating the effect of higher ones. Besides, Figure 5 shows the MCC tree reconstructing the evolutionary history of H3N2 Influenza, where each branch is colored with the air community where the corresponding lineage has spent more time. A quick inspection of the tree suggests that China and, in general, countries in Southern Asia were potential recurrent sources of infections. Indeed, their corresponding colors dominate the tree trunk, which we can here define as the sequence of external branches facing the top-right of the tree plot. To test this hypothesis, we compute the reward associated with each air community along the tree trunk; that is, the total expected time the CTMC spends in each of the states along the tree trunk (Minin and Suchard, 2007). The dot plot at the bottom of Figure 5 shows the posterior median trunk rewards associated with each air community using the GP model. In particular, the figure shows that the highest median trunk reward is associated with China (around 4 years between 2000 and 2007), confirming the aforementioned hypothesis.

5 Discussion

This work introduces a novel and more flexible framework for analyzing the influence of external covariates on the jump process of CTMCs, particularly addressing challenges in high-dimensional state spaces where direct parametrization is infeasible. Our primary contribution lies in relaxing the restrictive log-linear assumption prevalent in existing models by proposing a GP prior on a positive transformation of the infinitesimal rate matrix entries modeled as a random function of covariates. This formulation

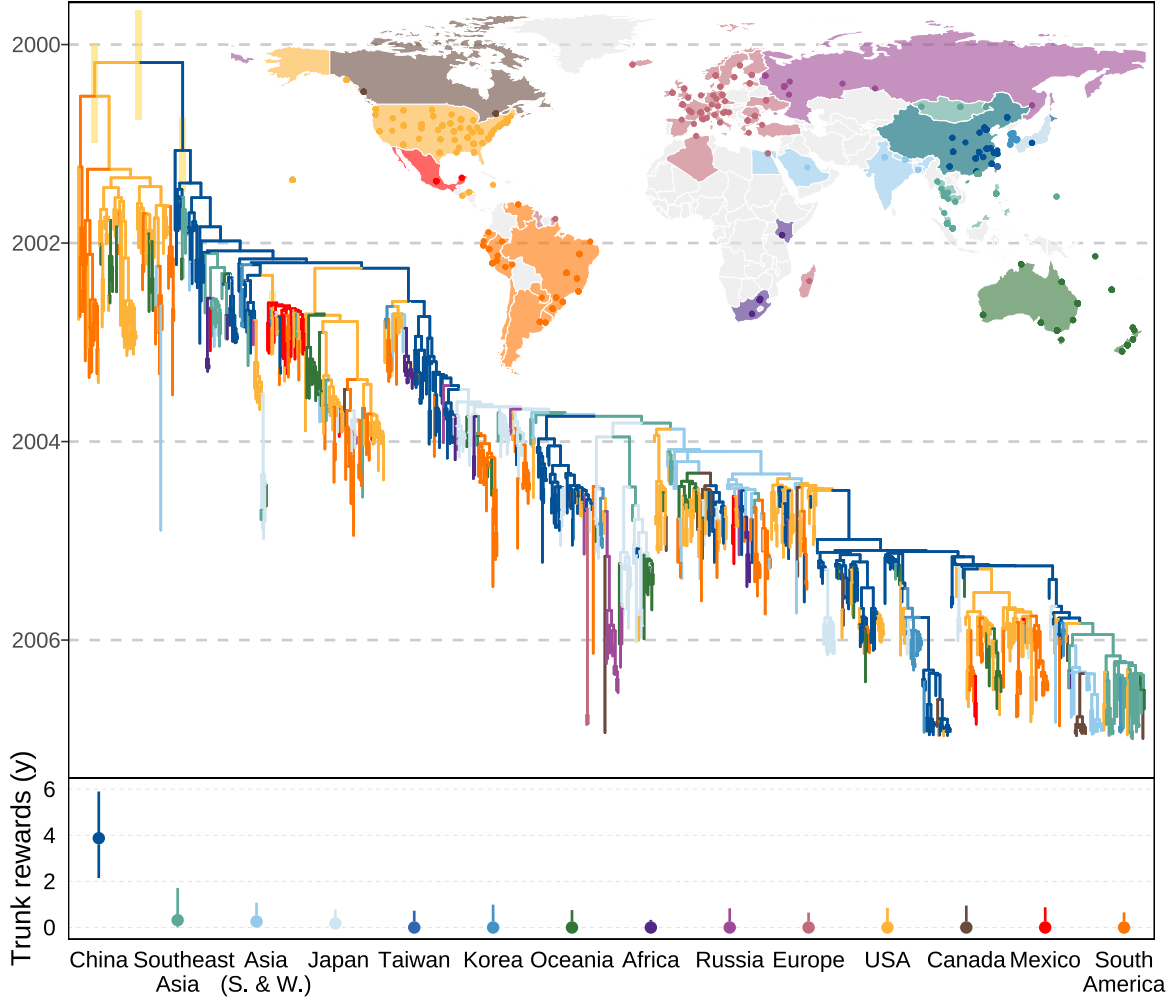


FIGURE 5: GLOBAL FLU DATA EXAMPLE

Note: Maximum clade credibility (MCC) tree showing the evolutionary history of H3N2 Influenza. The yellow bars placed on the internal nodes represent the 95% HPDIs for the node age. The different colors represent distinct air communities as represented on the map on the top-right, where the dots correspond to the analysed airports. Each branch color refers to the air community where the GP model predicts most time is spent. The dot plot with error bars on the bottom shows the trunk rewards in years based on the GP model. The trunk rewards accumulate the amount of time (in years) the CTMC spends in each state along the trunk, which in turn is defined as the set of external branches that face the top-right of the tree plot. The dot plot error bars show the 95% HPDIs.

allows transition rates to vary flexibly with covariates, thereby capturing a wide range of nonlinear relationships. Such flexibility is crucial in contexts where the structure of the underlying jump process is poorly understood.

A critical aspect of our methodology is the use of an efficient inferential scheme based on HMC with surrogate trajectories. Given the substantial computational burden associated with exact gradient computations for matrix exponentials in partially observed CTMCs, we leverage an approximation of the matrix exponential derivative (Didier et al., 2024). This approximation dramatically reduces the computational complexity of the log-posterior gradient from $\mathcal{O}(K^5)$ to $\mathcal{O}(K^2)$ with respect to all log-rates simultaneously, making inference tractable for larger state spaces. The theoretical underpinning provided by Li et al. (2019) ensures that, with a Metropolis-Hastings correction step, the exact posterior remains the stationary distribution of the Markov chain despite using an approximate gradient. Beyond methodological advances, we contribute directly to the field of Bayesian phylogenetics by integrating the proposed methods into the widely used BEAST X software. This implementation is intended to facilitate broader adoption within the scientific community and promote the exploration of covariate effects in phylogeographic models.

Our simulation study successfully validates the implementation within BEAST X, demonstrating the ability of the GP model to accurately recover the underlying log-rates, outperforming its log-linear counterpart when the true relationship is nonlinear. Two applications to real-world examples further illustrate the framework’s utility. In the analysis of bat rabies virus transmission, relaxing the log-linear assumption with a GP prior nevertheless supported a predominantly log-linear relationship between genetic distance and cross-species transmission rates. In contrast, for global seasonal influenza (H3N2) spread, the GP prior revealed that the log-linear model systematically misestimated the origin population density effects, overemphasizing the impact of low

population densities while underestimating that of higher ones. This example highlights how our GP framework can uncover subtle, nonlinear covariate effects that simpler models may obscure.

Future work could extend the framework to account for uncertainty in the covariates themselves, which are currently treated as fixed and known. Incorporating covariate uncertainty may yield more robust inference, particularly in settings where the external information is noisy or incomplete. Additionally, while the current approximation significantly enhances computational efficiency, further research could explore alternative scalable gradient approximations or inference strategies to support even larger or more complex state spaces.

In summary, the proposed framework offers a robust and scalable solution for Bayesian inference of CTMCs. By providing a principled way to model nonlinear covariate effects and employing computationally efficient gradient approximations, this work extends the capabilities of current models, allowing for deeper insights into the dynamics of stochastic processes.

Acknowledgments

The authors thank Moritz Kraemer and Philippe Lemey for insightful discussions and suggestions. We gratefully acknowledge support from Advanced Micro Devices, Inc. with the donation of parallel computing resources used for this research.

Funding

This work was supported through National Institutes of Health grants U19 AI135995, R01 AI153044 and R01 AI162611.

6 Appendix

6.1 Computing the tree-data likelihood gradient

To compute the gradient of the tree data likelihood with respect to the normalized rates, we leverage the chain rule to single out the contributions to the gradient of the rates specific to each branch and the $\boldsymbol{\pi}_{\text{root}}$. To accomplish this, we introduce a set of auxiliary branch- and rate-specific functions: $\eta_{uij}(\lambda_{ij}) = \lambda_{ij}$. Since $\boldsymbol{\pi}_{\text{root}}$ also possibly depends on all the rates, we extend the definition of the functions above such as $\eta_{2N-1,ij}(\lambda_{ij}) = \eta_{\text{root},ij}(\lambda_{ij}) = \lambda_{ij}$, where $2N - 1$ is the root node.

Therefore, substituting each rate at each branch and at the root with the corresponding auxiliary functions, we can apply the chain rule as follows:

$$\frac{\partial}{\partial \lambda_{ij}} = \sum_{u=1}^{2N-1} \frac{\partial}{\partial \eta_{uij}} \frac{\partial \eta_{uij}}{\partial \lambda_{ij}} = \sum_{u=1}^{2N-1} \frac{\partial}{\partial \eta_{uij}}, \quad (31)$$

where the second equality stems from $\frac{\partial \eta_{uij}}{\partial \lambda_{ij}} = 1$. Using this fact as well as the characterization of the tree data likelihood based on the pre- and post-order partial likelihood shown in Equation 25, and some further mathematical manipulations, we obtain

$$\begin{aligned} \frac{\partial p(\mathbf{y})}{\partial \lambda_{ij}} &= \sum_{u=1}^{2N-1} \frac{\partial p(\mathbf{y})}{\partial \eta_{uij}} = \sum_{u=1}^{2N-1} \frac{\partial}{\partial \eta_{uij}} \mathbf{p}'_u \mathbf{q}_u \\ &= \sum_{u=1}^{2N-2} \mathbf{p}'_u \frac{\partial}{\partial \eta_{uij}} \mathbf{P}(t_u)' [\mathbf{q}_{\text{pa}(u)} \circ \mathbf{P}(t_{\text{sibl}(u)}) \mathbf{p}_{\text{sibl}(u)}] + \mathbf{p}'_{2N-1} \frac{\partial}{\partial \lambda_{ij}} \boldsymbol{\pi}_{\text{root}} \\ &= \sum_{u=1}^{2N-2} \mathbf{p}'_u \frac{\partial}{\partial \eta_{uij}} \mathbf{P}(t_u)' \tilde{\mathbf{q}}_{\text{pa}(u)} + \mathbf{p}'_{2N-1} \frac{\partial}{\partial \lambda_{ij}} \boldsymbol{\pi}_{\text{root}} \\ &= \sum_{u=1}^{2N-2} \mathbf{p}'_u \left[\frac{\partial e^{t_u \boldsymbol{\Lambda}}}{\partial \eta_{uij}} \right]' \tilde{\mathbf{q}}_{\text{pa}(u)} + \mathbf{p}'_{2N-1} \frac{\partial}{\partial \lambda_{ij}} \boldsymbol{\pi}_{\text{root}} \\ &= \sum_{u=1}^{2N-2} \mathbf{p}'_u \left[\sum_{ab} \frac{\partial e^{t_u \boldsymbol{\Lambda}}}{\partial \lambda_{ab}} \frac{\partial \lambda_{ab}}{\partial \eta_{uij}} \right]' \tilde{\mathbf{q}}_{\text{pa}(u)} + \mathbf{p}'_{2N-1} \frac{\partial}{\partial \lambda_{ij}} \boldsymbol{\pi}_{\text{root}}, \end{aligned} \quad (32)$$

where the second line follows since \mathbf{p}_u does not depend on the branch connecting node u to its parent and by applying the pre-order pruning algorithm formula (27). Moreover, $\mathbf{p}'_{2N-1} \frac{\partial}{\partial \lambda_{ij}} \boldsymbol{\pi}_{\text{root}}$ represents the contribution to the derivative at the root node. In the third line, we define for notational convenience

$$\tilde{\mathbf{q}}_{\text{pa}(u)} := [\mathbf{q}_{\text{pa}(u)} \circ \mathbf{P}(t_{\text{sibl}(u)}) \mathbf{p}_{\text{sibl}(u)}] \quad (33)$$

and then notice that $\tilde{\mathbf{q}}_{\text{pa}(u)}$ does not depend on branch u . Finally, in the last two lines, we plug in the value of the finite-time transition matrix and we apply the chain rule to it. Noticing that $\frac{\partial \lambda_{ab}}{\partial \eta_{uij}} = 0$ when $ab \neq ij$ and $\frac{\partial \lambda_{ij}}{\partial \eta_{uij}} = 1$ we then reduce the expression above to:

$$\frac{\partial p(\mathbf{y})}{\partial \lambda_{ij}} = \sum_{u=1}^{2N-2} \mathbf{p}'_u \left[\frac{\partial e^{t_u \boldsymbol{\Lambda}}}{\partial \lambda_{ij}} \right]' \tilde{\mathbf{q}}_{\text{pa}(u)} + \mathbf{p}'_{2N-1} \frac{\partial}{\partial \lambda_{ij}} \boldsymbol{\pi}_{\text{root}}. \quad (34)$$

Bibliography

- Ayres, D. L., Cummings, M. P., Baele, G., Darling, A. E., Lewis, P. O., Swofford, D. L., Huelsenbeck, J. P., Lemey, P., Rambaut, A., and Suchard, M. A. (2019). BEAGLE 3: Improved Performance, Scaling, and Usability for a High-Performance Computing Library for Statistical Phylogenetics. *Systematic Biology*, 68(6):1052–1061.
- Baele, G., Carvalho, L. M., Brusselmans, M., Dudas, G., Ji, X., McCrone, J. T., Lemey, P., Suchard, M. A., and Rambaut, A. (2025a). HIPSTR: highest independent posterior subtree reconstruction in treeannotator x. *Bioinformatics*, pages 1–9.
- Baele, G., Ji, X., Hassler, G. W., McCrone, J. T., Shao, Y., Zhang, Z., Holbrook, A. J., Lemey, P., Drummond, A. J., Rambaut, A., and Suchard, M. A. (2025b). BEAST

- X for Bayesian phylogenetic, phylogeographic and phylodynamic inference. *Nature Methods*, pages 1–4.
- Baydin, A. G., Pearlmutter, B. A., Radul, A. A., and Siskind, J. M. (2018). Automatic Differentiation in Machine Learning: a Survey. *Journal of Machine Learning Research*, 18(153):1–43.
- Bielejec, F., Lemey, P., Carvalho, L. M., Baele, G., Rambaut, A., and Suchard, M. A. (2014). π BUSS: a parallel BEAST/BEAGLE utility for sequence simulation under complex evolutionary scenarios. *BMC Bioinformatics*, 15(1):133.
- Didier, G., Glatt-Holtz, N. E., Holbrook, A. J., Magee, A. F., and Suchard, M. A. (2024). On the surprising effectiveness of a simple matrix exponential derivative approximation, with application to global SARS-CoV-2. *Proceedings of the National Academy of Sciences*, 121(3):e2318989121.
- Duane, S., Kennedy, A. D., Pendleton, B. J., and Roweth, D. (1987). Hybrid Monte Carlo. *Physics Letters B*, 195(2):216–222.
- Duvenaud, D. K., Nickisch, H., and Rasmussen, C. (2011). Additive Gaussian Processes. In *Advances in Neural Information Processing Systems*, volume 24.
- Faria, N. R., Suchard, M. A., Rambaut, A., and Lemey, P. (2011). Toward a quantitative understanding of viral phylogeography. *Current Opinion in Virology*, 1(5):423–429.
- Faria, N. R., Suchard, M. A., Rambaut, A., Streicker, D. G., and Lemey, P. (2013). Simultaneously reconstructing viral cross-species transmission history and identifying the underlying constraints. *Philosophical Transactions of the Royal Society B: Biological Sciences*, 368(1614):20120196.

- Felsenstein, J. (1981). Evolutionary trees from DNA sequences: A maximum likelihood approach. *Journal of Molecular Evolution*, 17(6):368–376.
- Geman, S. and Geman, D. (1984). Stochastic relaxation, gibbs distributions, and the bayesian restoration of images. *IEEE Transactions on Pattern Analysis and Machine Intelligence*, 6(6):721–741.
- Hassler, G. W., Magee, A. F., Zhang, Z., Baele, G., Lemey, P., Ji, X., Fourment, M., and Suchard, M. A. (2023). Data Integration in Bayesian Phylogenetics. *Annual Review of Statistics and Its Application*, 10(1):353–377.
- Hastings, W. K. (1970). Monte Carlo sampling methods using Markov chains and their applications. *Biometrika*, 57(1):97–109.
- Jukes, T. H. and Cantor, C. R. (1969). Evolution of Protein Molecules. In *Mammalian Protein Metabolism*, pages 21–132. Elsevier.
- Kalbfleisch, J. D. and Lawless, J. F. (1985). The Analysis of Panel Data under a Markov Assumption. *Journal of the American Statistical Association*, 80(392):863–871.
- Kimura, M. (1980). A simple method for estimating evolutionary rates of base substitutions through comparative studies of nucleotide sequences. *Journal of Molecular Evolution*, 16(2):111–120.
- Lemey, P., Rambaut, A., Bedford, T., Faria, N., Bielejec, F., Baele, G., Russell, C. A., Smith, D. J., Pybus, O. G., Brockmann, D., and Suchard, M. A. (2014). Unifying Viral Genetics and Human Transportation Data to Predict the Global Transmission Dynamics of Human Influenza H3N2. *PLOS Pathogens*, 10(2):e1003932.

- Li, L., Holbrook, A., Shahbaba, B., and Baldi, P. (2019). Neural network gradient Hamiltonian Monte Carlo. *Computational statistics*, 34(1):281.
- Magee, A. F., Holbrook, A. J., Pekar, J. E., Caviedes-Solis, I. W., Matsen IV, F. A., Baele, G., Wertheim, J. O., Ji, X., Lemey, P., and Suchard, M. A. (2024). Random-Effects Substitution Models for Phylogenetics via Scalable Gradient Approximations. *Systematic Biology*, 73(3):562–578.
- Margossian, C. C. (2019). A review of automatic differentiation and its efficient implementation. *WIREs Data Mining and Knowledge Discovery*, 9(4):e1305.
- Metropolis, N., Rosenbluth, A. W., Rosenbluth, M. N., Teller, A. H., and Teller, E. (1953). Equation of State Calculations by Fast Computing Machines. *The Journal of Chemical Physics*, 21(6):1087–1092.
- Minin, V. N. and Suchard, M. A. (2007). Counting labeled transitions in continuous-time Markov models of evolution. *Journal of Mathematical Biology*, 56(3):391–412.
- Najfeld, I. and Havel, T. F. (1995). Derivatives of the Matrix Exponential and Their Computation. *Advances in Applied Mathematics*, 16(3):321–375.
- Neal, R. M. (2011). MCMC Using Hamiltonian Dynamics. In *Handbook of Markov Chain Monte Carlo*, pages 113–162. Chapman and Hall/CRC, New York, 1 edition.
- Pybus, O. G., Suchard, M. A., Lemey, P., Bernardin, F. J., Rambaut, A., Crawford, F. W., Gray, R. R., Arinaminpathy, N., Stramer, S. L., Busch, M. P., and Delwart, E. L. (2012). Unifying the spatial epidemiology and molecular evolution of emerging epidemics. *Proceedings of the National Academy of Sciences*, 109(37):15066–15071.
- Streicker, D. G., Turmelle, A. S., Vonhof, M. J., Kuzmin, I. V., McCracken, G. F., and

- Rupprecht, C. E. (2010). Host Phylogeny Constrains Cross-Species Emergence and Establishment of Rabies Virus in Bats. *Science*, 329(5992):676–679.
- Suchard, M. A., Weiss, R. E., and Sinsheimer, J. S. (2001). Bayesian Selection of Continuous-Time Markov Chain Evolutionary Models. *Molecular Biology and Evolution*, 18(6):1001–1013.
- Ward Jr., J. H. (1963). Hierarchical grouping to optimize an objective function. *Journal of the American Statistical Association*, 58(301):236–244.
- Zhao, T., Wang, Z., Cumberworth, A., Gsponer, J., Freitas, N. d., and Bouchard-Côté, A. (2016). Bayesian Analysis of Continuous Time Markov Chains with Application to Phylogenetic Modelling. *Bayesian Analysis*, 11(4):1203–1237.